

# Ultracold spin-balanced fermionic quantum liquids with renormalized $P$ -wave interactions

J. M. Alarcón\*

*Universidad de Alcalá, Grupo de Física Nuclear y de Partículas,  
Departamento de Física y Matemáticas, 28805 Alcalá de Henares (Madrid), Spain*

J. A. Oller†

*Departamento de Física, Universidad de Murcia, E-30071 Murcia, Spain.*

(Dated: July 20, 2021)

We consider spin-1/2 fermionic atoms whose dynamics are governed by low-energy  $P$ -wave interactions. These are renormalized within the ladder resummation scheme, and directly expressed as functions of the effective range parameters. Then, we show that, in a large scattering parameter regime, the zero-temperature equation of state exhibits a minimum, indicating the existence of a liquid phase. We also characterize the properties, such as the energy per particle, the compressibility or speed of sound of the liquid at equilibrium. The liquid exists near, but not strictly on, the unitary limit, which suggests the feasibility of realizing ultracold quantum liquids of fermions using  $P$ -wave Feshbach resonances.

The stability of liquids, whether classical or quantum-mechanical, stems from the competition between kinetic energy (temperature), repulsive and attractive forces [1, 2]. Near the absolute zero, attractive forces allow the constituent particles to stay close to each other – forming bound states – while repulsion, usually at short distances [3], avoids the collapse of the system in the thermodynamic limit. In the quantum case, it was recently shown theoretically [4], and subsequently observed experimentally [5–7], that certain bosonic systems can stably liquify at low temperatures thanks to one of the competing interactions arising from quantum fluctuations. Fermions, on the other hand, obey the Pauli principle, which acts as a natural mechanism for short-distance repulsion [8]. Therefore, attractive interactions on their own may stabilize fermionic quantum liquids.

Over the past decade or so, there have been tremendous advances in the manipulation and characterization of low-energy atom-atom interactions in the  $P$ -wave channel [9–12], their  $S$ -wave counterparts being well controlled and understood for some time now [13]. The effective low-energy  $P$ -wave interactions can be tuned essentially at will, including near resonance, where it may become the dominant interaction in the system, and certainly does for spin-polarized systems. An important, yet difficult question due to the non-perturbative nature of the interaction, is whether fermions near a  $P$ -wave resonance can form a stable liquid. In this Letter, we show that this is indeed the case, by resumming the ladder series of diagrams with an appropriate renormalization of the low-energy interaction, in the case of spin-balanced fermions. We find that, in a vast regime of scattering parameters, namely the  $P$ -wave volume  $a_1$  and effective range  $r_1$ , the zero-temperature equation of state exhibits

minima, corresponding to the equilibrium energy per particle, at the equilibrium density of the fermionic liquid. We also characterize other properties of the liquid, such as its equilibrium speed of sound, which can be measured using ultracold fermions [14].

Recently, Ref. [15] has derived a general compact expression for the calculation of the energy density for a spin-1/2 fermionic many-body system in the ladder approximation. The theory developed in Ref. [15] rests in the reformulation of many-body quantum field theory undertaken in Ref. [16], which determines the generating functional of Green functions in the fermionic many-body environment. See Ref. [17] for perturbative calculations up to next-to-leading order, and Ref. [18] for a recent review, considering also non-perturbative applications. We give here a brief account of the main features of this approach and refer to Ref. [15] for a detailed exposition.

The resummation of the Hartree and Fock diagrams, cf. Fig. 1, is done in terms of an arbitrary vacuum  $T$  matrix, called  $t_V$ , that includes both particle-particle and hole-hole intermediate states. The resulting expression for the energy density is

$$\mathcal{E} = \frac{k_F^5}{10m\pi^2} - \frac{i}{2} \text{Tr} \log (I - t_m L_d). \quad (1)$$

Above, the first term on the right-hand side is the kinetic energy of a non-interacting spin-1/2 Fermi gas, with Fermi momentum  $k_F$ , while the second term is the interaction energy. The trace there is taken over all two-fermion states *inside* the Fermi sea, that is, with momenta under  $k_F$  (this limitation is encoded in the loop function  $L_d$  to be specified below). In Eq. (1),  $t_m$  is an on-shell two-fermion scattering amplitude that we define after some preliminaries are introduced.

The expression for  $L_d$  is

$$L_d(p, \mathbf{a}) = i \frac{mp}{16\pi^2} \sum_{\sigma_1, 2} \int d\hat{\mathbf{k}} \theta(k_F - |\mathbf{a} + p\hat{\mathbf{k}}|) \theta(k_F - |\mathbf{a} - p\hat{\mathbf{k}}|) \times |p\hat{\mathbf{k}}\sigma_1\sigma_2\rangle_A \langle p\hat{\mathbf{k}}\sigma_1\sigma_2|. \quad (2)$$

\* jmanuel.alarcon@uah.es

† oller@um.es

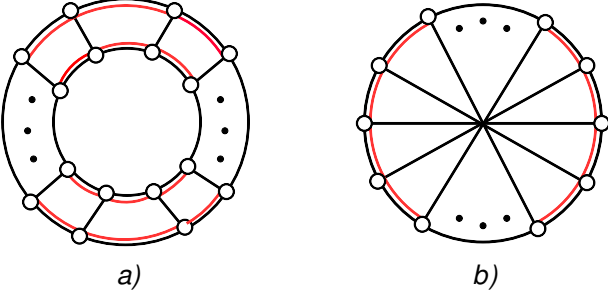


FIG. 1. Resummation of the Hartree (a) and Fock (b) diagrams. The black and red lines running in parallel are on-shell fermions with momenta less than  $k_F$ , and the  $L_d$  loops are given by two sets of such lines facing each other (Hartree) or radially opposite (Fock). The inwards single solid lines are  $t_m$ , and the dots indicate extra insertions of the interaction.

Above,  $|\mathbf{p}\sigma_1\sigma_2\rangle_A$  is an antisymmetric two-fermion state with third components of spin  $\sigma_i$ ,  $i = 1, 2$ , relative momentum  $\mathbf{p} \equiv (\mathbf{p}_1 - \mathbf{p}_2)/2$ , where  $\mathbf{p}_i$  is the momentum of the  $i^{\text{th}}$  particle. The total momentum is  $2\mathbf{a} \equiv \mathbf{p}_1 + \mathbf{p}_2$ . The Heaviside functions in Eq. (2) guarantee that the two fermions have momentum below  $k_F$ . The total energy of the on-shell pair is  $2a^0 = (\mathbf{p}_1^2 + \mathbf{p}_2^2)/2m = (\mathbf{a}^2 + \mathbf{p}^2)/m$ , which fixes  $p \equiv |\mathbf{p}|$  for a given total momentum (since  $\mathbf{a}$  is conserved in the scattering process).

The in-medium scattering amplitude  $t_m(\mathbf{a})$  stems from the iteration  $t_V$  with *mixed* two-fermion intermediate states in which one of them has momentum below  $k_F$  while the momentum of the other one is unconstrained. The loop function associated to these intermediate states is  $L_m(p, \mathbf{a})$ . The explicit expression for  $L_m$  is

$$L_m(p, \mathbf{a}) = -\frac{m}{2} \sum_{\sigma_{1,2}} \int \frac{d\mathbf{k}}{(2\pi)^3} [\theta(k_F - |\mathbf{a} + \mathbf{k}|) + \theta(k_F - |\mathbf{a} - \mathbf{k}|)] \frac{|\mathbf{k}\sigma_1\sigma_2\rangle_A \langle \mathbf{k}\sigma_1\sigma_2|}{\mathbf{k}^2 - \mathbf{p}^2 - i\epsilon}. \quad (3)$$

The amplitude  $t_m(\mathbf{a})$  satisfies the following equation,

$$t_m(\mathbf{a}) = t_V + t_V L_m(p, \mathbf{a}) t_m(\mathbf{a}). \quad (4)$$

In Fig. 1, we draw the diagrams resummed by the interacting part of  $\mathcal{E}$  in Eq. (1). The Hartree diagrams are shown in Fig. 1(a) and the Fock ones in 1(b). The double lines (one in black and another in red running parallel to each other) are fermions inside the Fermi sea, while a single solid line corresponds to an in-medium interaction  $t_m$ . Notice that in the Hartree diagrams two facing sets of double lines made up a  $L_d$ , while for the Fock diagrams this is so for radially opposite double lines. The intermediate states in  $L_d$  interact by  $t_m$ , and the three dots indicate further iterations of the product  $t_m L_d$ .

The evaluation of the interaction energy is done using the partial-wave expansion developed in Ref. [15]. The states in the partial-wave basis are denoted by  $|J\mu p S\rangle$ ,

with definite total angular momentum  $J$ , third component  $\mu$ , orbital angular momentum  $\ell$  and total spin  $S$ . By taking the trace in Eq. (1) in the plane-wave basis one has

$$\mathcal{E} = \frac{k_F^5}{10m\pi^2} - \frac{2i}{m\pi^3} \sum_{J\mu\ell S} \chi(S\ell)^2 \int_0^\infty p dp \int_0^\infty a^2 da \quad (5) \\ \times \langle J\mu\ell S p | \log(I - t_m(a\hat{\mathbf{z}}) L_d(p, a\hat{\mathbf{z}})) | J\mu\ell S p \rangle,$$

where rotational invariance allows to take  $\mathbf{a}$  along the  $z$  axis. The factor  $\chi(S\ell)^2$  selects even values for the sum  $S + \ell$  because of the Pauli exclusion principle, being 2 in that case.

The integral equation satisfied by the partial-wave amplitudes (PWAs) in the many-body environment is more involved than in the vacuum case because of the extra mixing between PWAs due to the dependence of scattering on the total momenta. This extra mixing is accounted for within the formalism by the matrix

$$\mathcal{B}_{J_2\mu\ell_2, J_1\mu\ell_1} = -2\chi(S\ell_2)\chi(S\ell_1) \sum_{m_3 s_3} (m_3 s_3 \mu | \ell_2 S J_2) \quad (6) \\ \times (m_3 s_3 \mu | \ell_1 S J_1) \int d\hat{\mathbf{k}} Y_{\ell_2}^{m_3}(\hat{\mathbf{k}})^* Y_{\ell_1}^{m_3}(\hat{\mathbf{k}}) \theta(k_F - |\mathbf{k} - a\hat{\mathbf{z}}|).$$

However,  $\mu$  and  $S$  are conserved in the scattering process [15]. In the previous equation  $Y_\ell^m(\hat{\mathbf{k}})$  is a spherical harmonic and  $(m_1 m_2 m_3 | j_1 j_2 j_3)$  is the Clebsch-Gordan coefficient for the addition of the angular momenta  $\mathbf{j}_1 + \mathbf{j}_2 = \mathbf{j}_3$ .

For the case of contact interactions it is shown in Ref. [15] that it is possible to derive an algebraic expression for the vacuum off-shell PWAs  $t_V(p', p)_{\alpha\beta}$  for  $p, p'$  bounded (this is the case in the integral equation of Eq. (4), where  $p$  and  $p' < 2k_F$ ). Using a cutoff regularization in a generic scheme these PWAs are renormalized by reproducing the effective-range expansion (ERE) up to some order, with the cutoff finally sent to infinity. Within a matrix notation, so that the set of coupled PWAs is denoted by the matrix  $t_V(p', p)$ , one can show that

$$t_V(p', p) = \frac{4\pi}{m} (p')^\ell \tau(p) (p)^\ell, \quad (7) \\ (p)^\ell = \text{diag}(p^{\ell_1}, \dots, p^{\ell_n}),$$

and analogously for  $(p')^\ell$ . In the previous equation,  $\ell_i$  ( $i = 1, \dots, n$ ) is the orbital angular momentum of the  $n$  coupled PWAs, and

$$\tau(p)^{-1} = -(a)^{-1} + \frac{1}{2}(r)p^2 + \sum_{i=2}^M (v_\ell^{(2i)}) p^{2i} - i(p^\ell)^2(p), \quad (8)$$

with  $M$  the order up to which the ERE is reproduced. In this equation  $(a)$ ,  $(r)$  and  $(v_\ell^{(2i)})$  are  $n \times n$  matrices corresponding to the scattering length, effective range and shape parameters, respectively[19]. We note that a minimum value of  $M$ , depending on the PWAs studied,

is needed to achieve renormalizability. E.g. in the case of  $P$  wave scattering, considered here, one needs at least  $M = 2$ .

In terms of this expression, and using an analogous matrix notation for the set of PWAs in the many-body environment,

$$\begin{aligned} \mathbf{t}_m(p, p) &= \frac{4\pi}{m} (p^\ell) (\tau(p)^{-1} + [\mathcal{G}_m(p)])^{-1} (p^\ell), \\ [\mathcal{G}_m(p)] &= -\frac{1}{\pi} \int_0^\infty \frac{k^2 dk}{k^2 - p^2 - i\epsilon} (k^\ell) \cdot \mathcal{B} \cdot (k^\ell). \end{aligned} \quad (9)$$

Now, we proceed to apply the previous formalism to a liquid interacting via a spin-independent  $P$ -wave potential  $v(k, p) = \mathbf{k} \cdot \mathbf{p} (d_0 + d_2(k^2 + p^2))$ , with the parameters  $d_0$  and  $d_2$  given in terms of the cutoff to reproduce the ERE up to and including the effective range. For this interaction the ERE simplifies since  $(a)$ ,  $(r)$ , and  $(v_1^{2i})$  in Eq. (8) become just parameters equal to  $a_1$ ,  $r_1$  and  $v_1^{2i}$ , respectively, as the scattering in vacuum is uncoupled. Had we used dimensional regularization, as in Refs. [20, 21], instead of cutoff regularization [22], a renormalized result is possible reproducing only the scattering volume. However, as we argue in [15], we interpret it as an artifact of dimensional regularization in non-perturbative calculations because, as it is well known, the power-like divergences are set to zero in this particular regularization method [23].

In the case of a  $P$ -wave interaction ( $\ell = 1$ ) of two identical fermions, Fermi statistics requires that  $S = 1$ , and for each  $\mu$  only the PWAs with  $J \geq |\mu|$  contribute. For  $\mu = 0$  we have the mixing between the PWAs  $^3P_0$  and  $^3P_2$ , while  $^3P_1$  does not couple. In the case with  $\mu = \pm 1$  the mixing is between  $^3P_1$  and  $^3P_2$ , and for  $\mu = \pm 2$  only the  $^3P_2$  contributes. One can solve directly for  $\mathbf{t}_m(p, p)$  in this case and in terms of it calculate the energy density  $\mathcal{E}$  applying Eq. (1). The evaluation of the trace of the log is performed by diagonalizing the matrix in its argument which is possible because it is a unitary matrix. The detailed full calculation is undertaken in Ref. [15].

We study the energy per particle  $\bar{\mathcal{E}} = \mathcal{E}/\rho$ , where  $\rho = k_F^3/3\pi^2$  is the number density, as a function of the scattering length  $a_1$  and the effective range  $r_1$ . The dimensionless variables  $x = -1/a_1 r_1^3$  and  $y = k_F/r_1$  are introduced, so that  $\bar{\mathcal{E}} = \frac{3k_F^2}{10m} f(x, y) = r_1^2 \frac{3y^2}{10m} f(x, y)$ . To look for the minima of  $\bar{\mathcal{E}}$  when varying  $k_F$  for given values of  $a_1$  and  $r_1$  it is advantageous to consider the new coordinates  $u = \tanh(x)$  and  $v = \tanh(y)$ , and then the whole plane  $xy$  is compressed to the finite extent  $(-1, 1) \otimes (-1, 1)$  in the  $uv$  plane. The minimum of  $\bar{\mathcal{E}}$  has to be searched along the  $v$  axis because when  $k_F$  changes  $u$  stays put. We look for them numerically in steps of  $10^{-3}$  in the  $v$  variable for a given  $u$ . Numerical inaccuracy prevents us from taking smaller steps, which could *a priori* limit our search for potentially narrow, yet physical minima.

The energy per particle, in kelvin,  $\bar{\mathcal{E}}/k_B$ , with  $k_B$  the

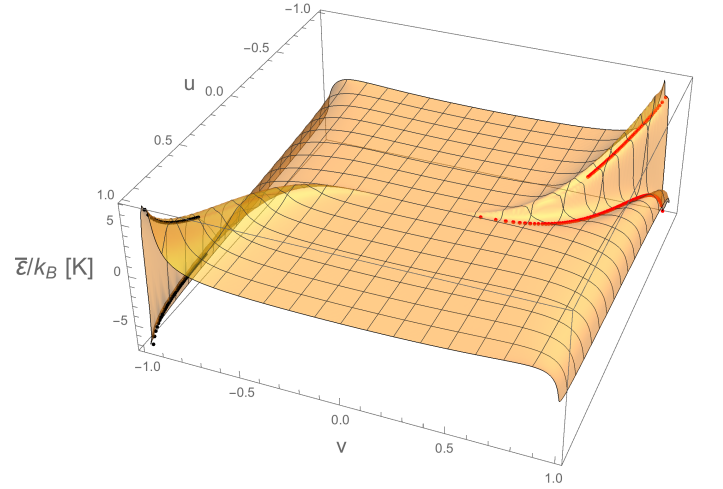


FIG. 2. The energy per particle  $\bar{\mathcal{E}}$  in units of kelvin is plotted in the  $uv$  plane. The positions of the minima are also indicated by the dots on top of the surface.

Boltzmann constant, is plotted in Fig. 2 in the  $uv$  plane. The filled dots in the same figure mark the positions of the minima. The value of  $\bar{\mathcal{E}}$  in absolute terms results by taking, for concreteness,  $|r_1| = 0.28 a_B^{-1}$  [11] and  $m$  for  $^6\text{Li}$  scattering, with  $a_B$  the Bohr radius [24]. Notice that the sign of  $r_1$  does not affect  $\bar{\mathcal{E}}$  since, as indicated above,  $\bar{\mathcal{E}} = r_1^2 \frac{3y^2}{10m} f(x, y)$ . In Fig. 2, we observe four branches of minima within the whole set of parametric values for  $a_1$  and  $r_1$ , two with  $\bar{\mathcal{E}} > 0$  and the other two with  $\bar{\mathcal{E}} < 0$ . Among all of them, and within our numerical precision, only one branch can approach arbitrarily close to the unitary limit at  $u = v = 0$  (*i.e.*  $|a_1|, |r_1| \rightarrow \infty$ , and  $k_F \rightarrow 0$ ), though never strictly on it. This is the longest branch in the top right corner in Fig. 2. Indeed, as we have checked explicitly, the minimum for  $u = 0$  happens at  $k_F = 0$ . The other branches only happen for values of  $|u|$  large enough that, for a given  $r_1$ , implies a maximum value for  $|a_1|$ , and stay away from the unitary limit.

From the calculation of  $\bar{\mathcal{E}}$  we can obtain other thermodynamic and mechanical properties of the minima by employing well-known thermodynamic identities. At the minimum the pressure  $P$  vanishes, while the chemical potential  $\mu$  is simply  $\bar{\mathcal{E}}$ . We also consider the sound velocity  $c_s$  and the coefficient of compressibility  $K$ . At a minimum of  $\bar{\mathcal{E}}$  these magnitudes fulfill the relations

$$\begin{aligned} c_s^2 &= \frac{\partial P}{\partial \rho(m + \bar{\mathcal{E}})} = \frac{1}{m + \bar{\mathcal{E}}} \frac{\partial}{\partial \rho} \left( \rho^2 \frac{\partial \bar{\mathcal{E}}}{\partial \rho} \right), \\ K^{-1} &= c_s^2 \rho (m + \bar{\mathcal{E}}). \end{aligned} \quad (10)$$

Another interesting relation is that  $K^{-1} = \rho^2 \frac{\partial \mu}{\partial \rho}$ , so that the derivative of the chemical potential with respect to the density is positive at the minima.

The calculated properties of the minima are plotted in Figs. 3 ( $\bar{\mathcal{E}} < 0$ ) and 4 ( $\bar{\mathcal{E}} > 0$ ), calculated with the

sign of  $r_1$  chosen such that  $r_1 v > 0$ , because then  $k_F = r_1 \operatorname{arctanh} v > 0$  as it must (notice that for the minima  $uv < 0$ ). From top to bottom and left to right, we plot  $a_1$ ,  $\rho$  (both in units of  $a_B^{-3}$ ),  $\bar{\mathcal{E}}$  in kelvin,  $c_s$  in  $m/s$ , the ratio  $c_s/v_F$ , where  $v_F = k_F/m$  is the Fermi velocity, and  $K/K_{\text{free}}$ , with  $K_{\text{free}} = \frac{k_F^5}{9\pi^2}$  the compressibility coefficient for a free Fermi gas.

In Fig. 3 the minima with  $\bar{\mathcal{E}} < 0$  are considered. The left branch when approaching the unitary limit has a clear gas behavior with diverging  $K$  and vanishing  $\rho$ ,  $\bar{\mathcal{E}}$  and  $c_s$  in that limit. The other branch has a maximum value for  $a_1$  of  $67.2 a_B^{-1}$ . For the branches with  $\bar{\mathcal{E}} > 0$  drawn in Fig. 4 their scattering volumes are also bounded from above with the maxima values of  $a_1 = 101.8 a_B^{-1}$  for  $u < 0$ , and  $49.0 a_B^{-1}$  for  $u > 0$ . In both figures we observe that the density of particles has typical values of a few fermions in a volume of  $10^3 a_B^3$ . The sound velocity shows typical values of hundreds of  $m/s$  and, except in the case of diverging  $a_1$ , it is larger than  $v_F$ .

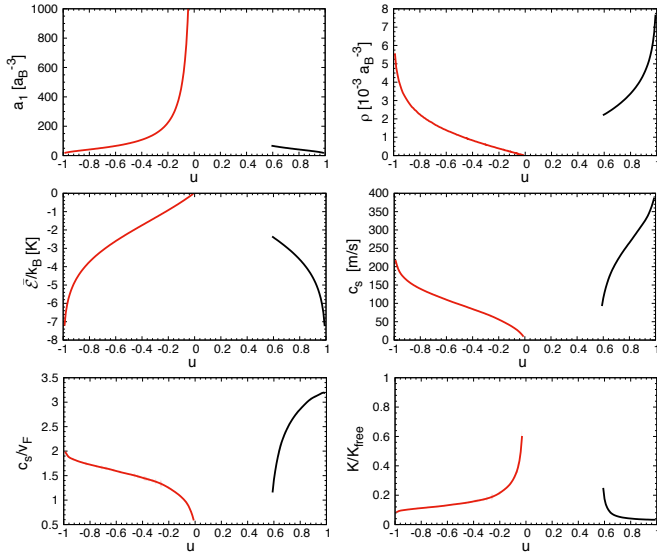


FIG. 3. Properties for the minima with  $\bar{\mathcal{E}} < 0$ . From top to bottom and left to right  $a_1 [a_B^{-3}]$ ,  $\rho [a_B^{-3}]$ ,  $\bar{\mathcal{E}}_B [K]$ ,  $c_s [m/s]$ ,  $c_s/v_F$  and  $K/K_{\text{free}}$  are plotted.

Let us consider closely the unitary limit with  $x = 0$  and work out the leading behavior in powers of  $y$  of  $f(0, y) = \bar{\mathcal{E}} \frac{10m}{3k_F^2}$  as introduced above. To calculate  $\bar{\mathcal{E}}$  we have the dimensionless combination  $1 - \mathfrak{t}_m L_d$  inside a log, cf. Eq.(1). In  $k_F^3 \tau(k_F)$  we can extract a global dimensionless factor  $y^3 = (k_F/r_1)^3$  and the rest adopts the form  $\left(x + \frac{1}{2}y^2 + v_1^{(2)} r_1 y^4 - i y^3 + \mathcal{O}(y^4)\right)^{-1}$ , with  $x = 0$  in the unitary limit. We indicate the real and imaginary parts of  $\mathfrak{t}_m$  and  $L_d$  as  $\mathfrak{t}_m^r$ ,  $\mathfrak{t}_m^i$ , and  $L_d^r$ ,  $L_d^i$ , respectively. Therefore,  $\mathfrak{t}_m^r L_d^i$  is proportional to  $y$  while  $1 - i \mathfrak{t}_m^i L_d^i$  behaves as  $1 + \mathcal{O}(y^2)$ , so that  $\arctan(\mathfrak{t}_m^r L_d^i / (1 - i \mathfrak{t}_m^i L_d^i)) \sim y$ . We can then write  $\bar{\mathcal{E}} = \frac{3k_F^2}{10m} (1 + \xi_1 y)$ , for  $x = 0$  and

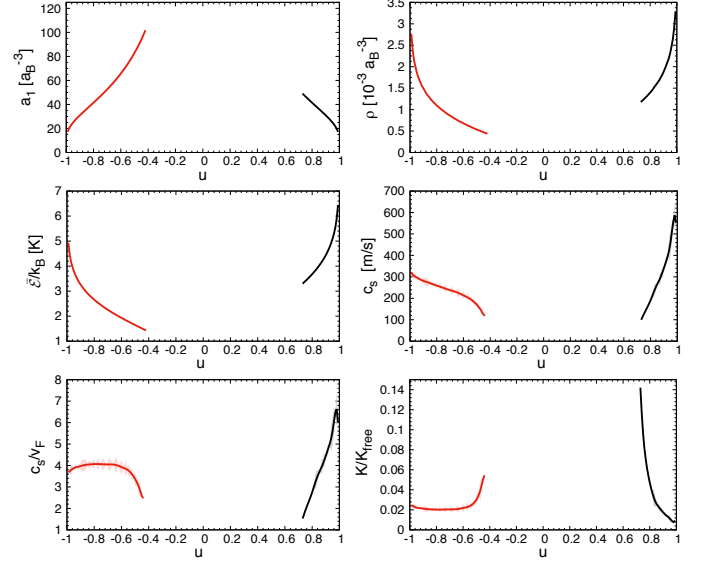


FIG. 4. Properties for the minima with  $\bar{\mathcal{E}} > 0$ . The light shaded areas reflect the remaining numerical uncertainty in our calculation. For the rest see the caption in Fig. 3.

$|y| \ll 1$ . Because of the non-perturbative contribution of the effective-range parameter the unitary limit depends on the order in which the limits  $x \rightarrow 0$  and  $y \rightarrow 0$  are taken. Following an analogous procedure as before it results that for  $|y/x| \ll 1$  the function  $f(x, y)$  behaves as  $(1 + \xi_2 y^3/x + \xi_3 y^5/x^2)$ , where both  $\xi_2$  and  $\xi_3$  are universal since the higher-order shape parameters in the ERE, starting from  $v_1^{(2)}$ , are  $\mathcal{O}(y^7)$ . Our calculation predicts the following values for these universal parameters

$$\xi_1 = -6.4054, \quad \xi_2 = -0.9549, \quad \xi_3 = 0.2049. \quad (11)$$

In summary, we have performed a non-perturbative renormalized calculation for fermionic quantum liquids interacting with pure  $P$ -wave spin independent interactions. A rich structure of minima has been predicted in the whole parametric set of values for  $a_1$  and  $r_1$ . Out of the four branches of minima that result, one of them reaches values close to (but not strictly at) the unitary limit. Our results indicate where to look for the experimental realization of these quantum liquids using ultra-cold fermionic atoms in a  $P$ -wave Feshbach resonance. It would also be interesting to apply these methods to other systems such unbalanced-spin quantum liquids and/or interacting with higher partial waves.

## ACKNOWLEDGEMENTS

We are grateful to Manuel Valiente for bringing this problem to our attention, for many useful discussions, his participation in the writing of the introduction and a critical reading of the manuscript. This work has been supported in part

by the MICINN AEI (Spain) Grants PID2019-

106080GB-C21/AEI/10.13039/501100011033 and  
PID2019-106080GB-C22/AEI/10.13039/501100011033.

- 
- [1] J. P. Hansen and I. R. McDonald, *Theory of Simple Liquids* (Academic Press, Oxford, 2013).
  - [2] A. Leggett, *Quantum Liquids: Bose Condensation and Cooper Pairing in Condensed-Matter Systems* (Oxford University Press, Oxford, 2006).
  - [3] R. A. Aziz and M. J. Slaman, *J. Chem. Phys.* **94**, 8047 (1991).
  - [4] D. S. Petrov, *Phys. Rev. Lett.* **115**, 155302 (2015).
  - [5] C. R. Cabrera, L. Tanzi, J. Sanz, B. Naylor, P. Thomas, P. Cheiney, and L. Tarruell, *Phys. Rev. Lett.* **115**, 155302 (2015).
  - [6] P. Cheiney, C. R. Cabrera, J. Sanz, B. Naylor, L. Tanzi, and L. Tarruell, *Phys. Rev. Lett.* **120**, 135301 (2018).
  - [7] G. Semeghini, G. Ferioli, L. Masi, C. Mazzinghi, L. Wolswijk, F. Minardi, M. Modugno, G. Modugno, M. Inguscio, and M. Fattori, *Phys. Rev. Lett.* **120**, 235301 (2018).
  - [8] A. Fetter and J. Walecka, *Quantum Theory of Many-Particle Systems* (McGraw-Hill, New York, 1971).
  - [9] J. Zhang, E. G. M. van Kempen, T. Bourdel, L. Khaykovich, J. Cubizolles, F. Chevy, M. Teichmann, L. Tarruell, S. J. J. M. F. Kokkelmans, and C. Salomon, *Phys. Rev. A* **70**, 030702(R) (2004).
  - [10] S. Dong, Y. Cui, C. Shen, Y. Wu, M. K. Tey, L. You, and B. Gao, *Phys. Rev. A* **94**, 062702 (2016).
  - [11] Y. T. Chang, R. Senaratne, D. Cavazos-Cavazos, and R. G. Hulet, *Phys. Rev. Lett.* **125**, 263402 (2020).
  - [12] A. S. Marcum, F. R. Fonta, A. M. Ismail, and K. M. O'Hara, (2020), [arXiv:2007.15783 \[physics.atom-ph\]](#).
  - [13] C. Chin, R. Grimm, P. Julienne, and E. Teisinga, *Rev. Mod. Phys.* **82**, 1225 (2010).
  - [14] J. Joseph, B. Clancy, L. Luo, J. Kinast, T. A., and J. E. Thomas, *Phys. Rev. Lett.* **98**, 170401 (2007).
  - [15] J. M. Alarcón and J. A. Oller, [arXiv:2106.02652 \[nucl-th\]](#).
  - [16] J. Oller, *Phys. Rev. C* **65**, 025204 (2002), [arXiv:hep-ph/0101204](#).
  - [17] U. G. Meissner, J. A. Oller, and A. Wirzba, *Annals Phys.* **297**, 27 (2002), [arXiv:nucl-th/0109026](#).
  - [18] J. A. Oller, *J. Phys. G* **46**, 073001 (2019), [arXiv:1902.06065 \[nucl-th\]](#).
  - [19] Depending of the PWAs the dimension of the entries in  $(a)$ ,  $(r)$ , etc, are different. We always use the same name for simplicity.
  - [20] N. Kaiser, *Eur. Phys. J. A* **48**, 148 (2012), [arXiv:1210.0783 \[nucl-th\]](#).
  - [21] N. Kaiser, *Nucl. Phys. A* **860**, 41 (2011), [arXiv:1102.2154 \[nucl-th\]](#).
  - [22] U. van Kolck, *Nucl. Phys. A* **645**, 273 (1999), [arXiv:nucl-th/9808007](#).
  - [23] See also Refs. [25, 26] for further discussions and more examples in vacuum scattering.
  - [24] Within our conventions the effective range is multiplied by a factor  $-2$  compared to [11].
  - [25] D. R. Phillips, S. R. Beane, and T. D. Cohen, *Annals Phys.* **263**, 255 (1998), [arXiv:hep-th/9706070](#).
  - [26] J. Oller, *Annals Phys.* **396**, 429 (2018), [arXiv:1710.00991 \[hep-ph\]](#).